

Supplementary Materials

to the manuscript:

Bioengineered lipophilic Ru(III) complexes as potential anticancer agents

Claudia Riccardi,^a Marialuisa Piccolo,^b Maria Grazia Ferraro,^b Raffaele Graziano,^{a,b}
Domenica Musumeci,^{a,c} Marco Trifuggi,^a Carlo Irace,^b Daniela Montesarchio^{a,*}

^a Department of Chemical Sciences, University of Naples “Federico II”, Via Cintia 21, 80126 Naples, Italy

^b Department of Pharmacy, School of Medicine and Surgery, University of Naples “Federico II”, Via D. Montesano 49, 80131 Naples, Italy

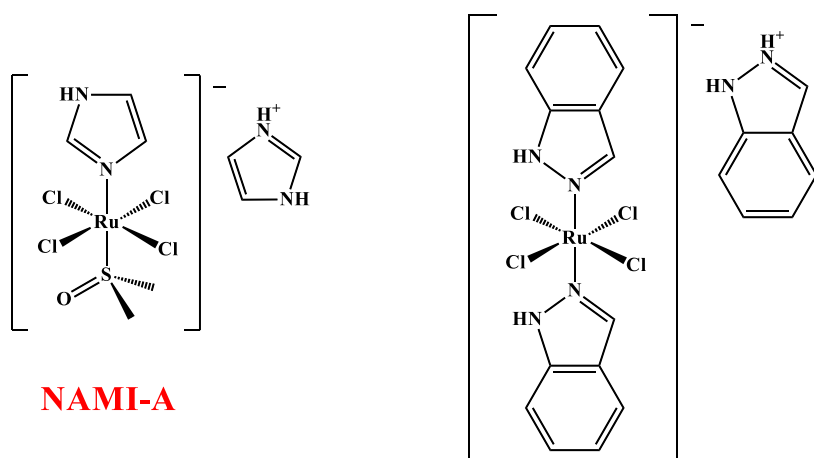
^c Institute of Biostructures and Bioimages, CNR, Naples, Italy

*Author to whom correspondence should be addressed.

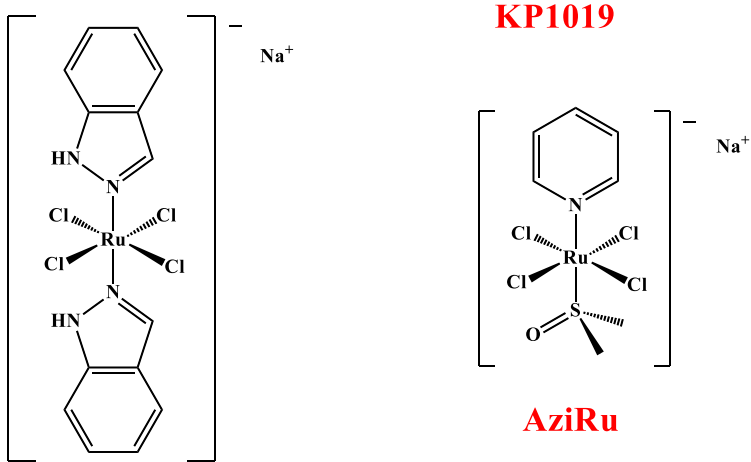
e-mail address: daniela.montesarchio@unina.it

Table of contents.

Figure S1. Chemical structures of previously reported Ru(III) complexes	pag. S1
Figure S2. TLC analysis of pure lipophilic pyridine derivatives and Ru(III) complexes	pag. S2
Figure S3. Chemical structures of the here proposed lipophilic Ru(III) complexes	pag. S3
Figure S4. ESI-MS spectra of lipophilic pyridine derivatives	pag. S4
Figure S5. ESI-MS spectra of lipophilic Ru(III) complexes	pag. S5
Figure S6. ESI-MS spectrum of PalmiPyRu and peak isotopic distribution	pag. S6
Figure S7. UV-vis absorption spectra recorded in DMSO	pag. S7
Table S1. Absorbance maxima values derived from UV analysis	pag. S8
Figure S8. UV-vis-monitored hydrolysis experiments: absorbance spectra over time	pag. S9
Figure S9. UV-vis-monitored hydrolysis experiments: evaluation of the $t_{1/2}$ values	pag. S10
Figure S10. Size distribution by intensity of lipophilic Ru(III) complexes	pag. S11
Table S2. DLS analysis over time of lipophilic Ru(III) complexes	pag. S12
Figure S11. Size distribution by intensity and DLS analysis over time of PalmiPyRu	pag. S13
Figure S12. Cell viability assays	pag. S14
Figure S13. CD analysis of the selected DNA model systems	pag. S15
Figure S14. CD experiments with the duplexGG	pag. S16
Figure S15. CD experiments with the G-quadruplex Pu22T14T23	pag. S17
Figure S16. Stern-Volmer plots of fluorescence experiments	pag. S18
Table S3. Stern-Volmer quenching constants determination	pag. S19
Figure S17. Double logarithmic plots of fluorescence experiments	pag. S20
Table S4. Binding parameter determination	pag. S21
Figure S18. Nomenclature used in the description of NMR spectra	pag. S22
Figure S19. ^1H and ^{13}C NMR spectra of PalmiPy	pag. S23
Figure S20. ^1H - ^1H COSY and HSQC NMR spectra of PalmiPy	pag. S24

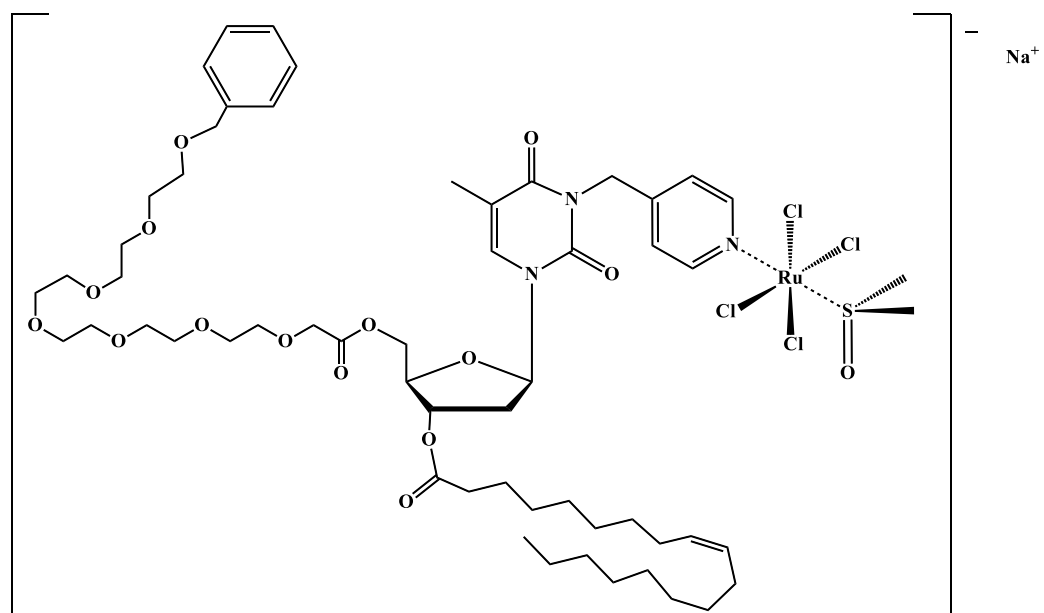


KP1019



AziRu

NKP1339



HoThyRu

Figure S1. Chemical structures of NAMI-A, KP1019, NKP-1339, AziRu and HoThyRu, as indicated.

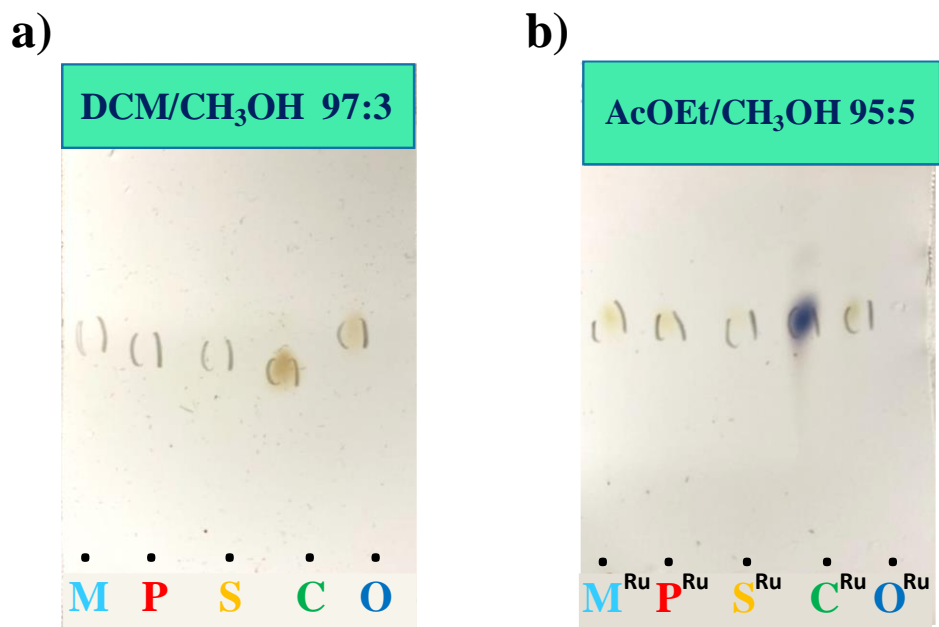


Figure S2. Representative TLC analysis of pure lipophilic (a) pyridine derivatives and (b) Ru(III) complexes, as observed in the DCM/CH₃OH (97:3, v/v) and ethyl acetate/CH₃OH (95:5, v/v) eluent mixtures, respectively. Reaction products on TLC plates were first visualized by UV light and then by gently heating after treatment with an oxidant acidic solution (acetic acid / water / sulfuric acid, 10:4:5, v/v), as indicated in the experimental section. [M=MyriPy, P=PalmiPy, S=StePy, C=CholPy, O=OlePy].

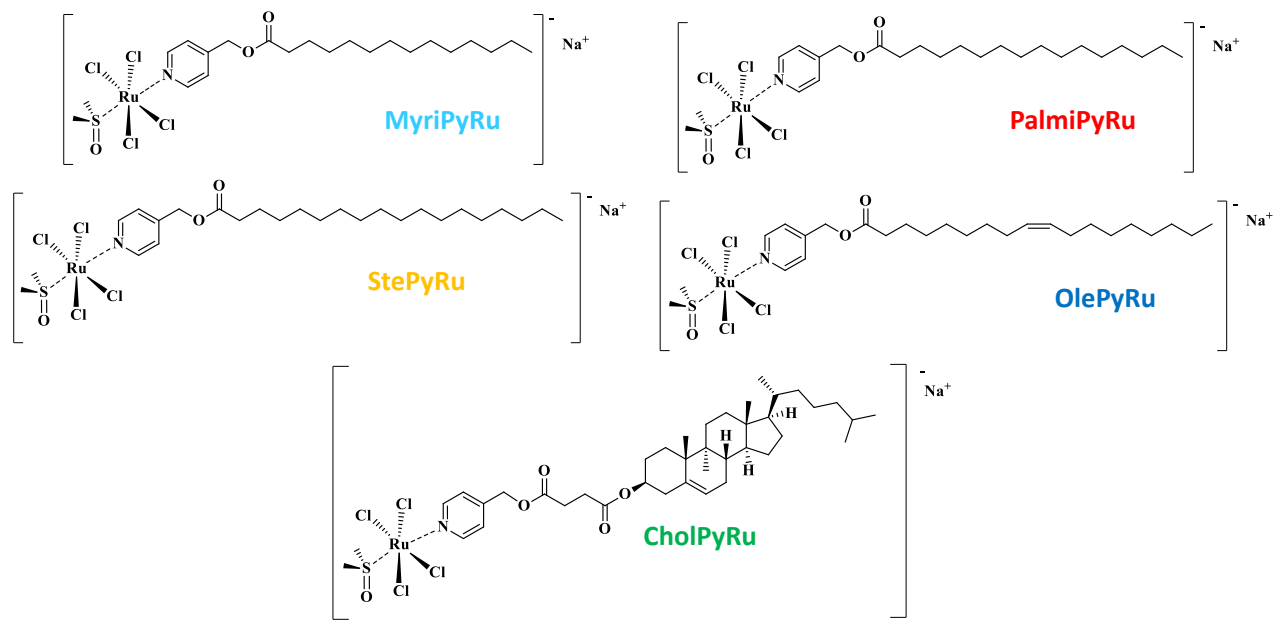


Figure S3. Chemical structures of the here proposed lipophilic Ru(III) complexes.

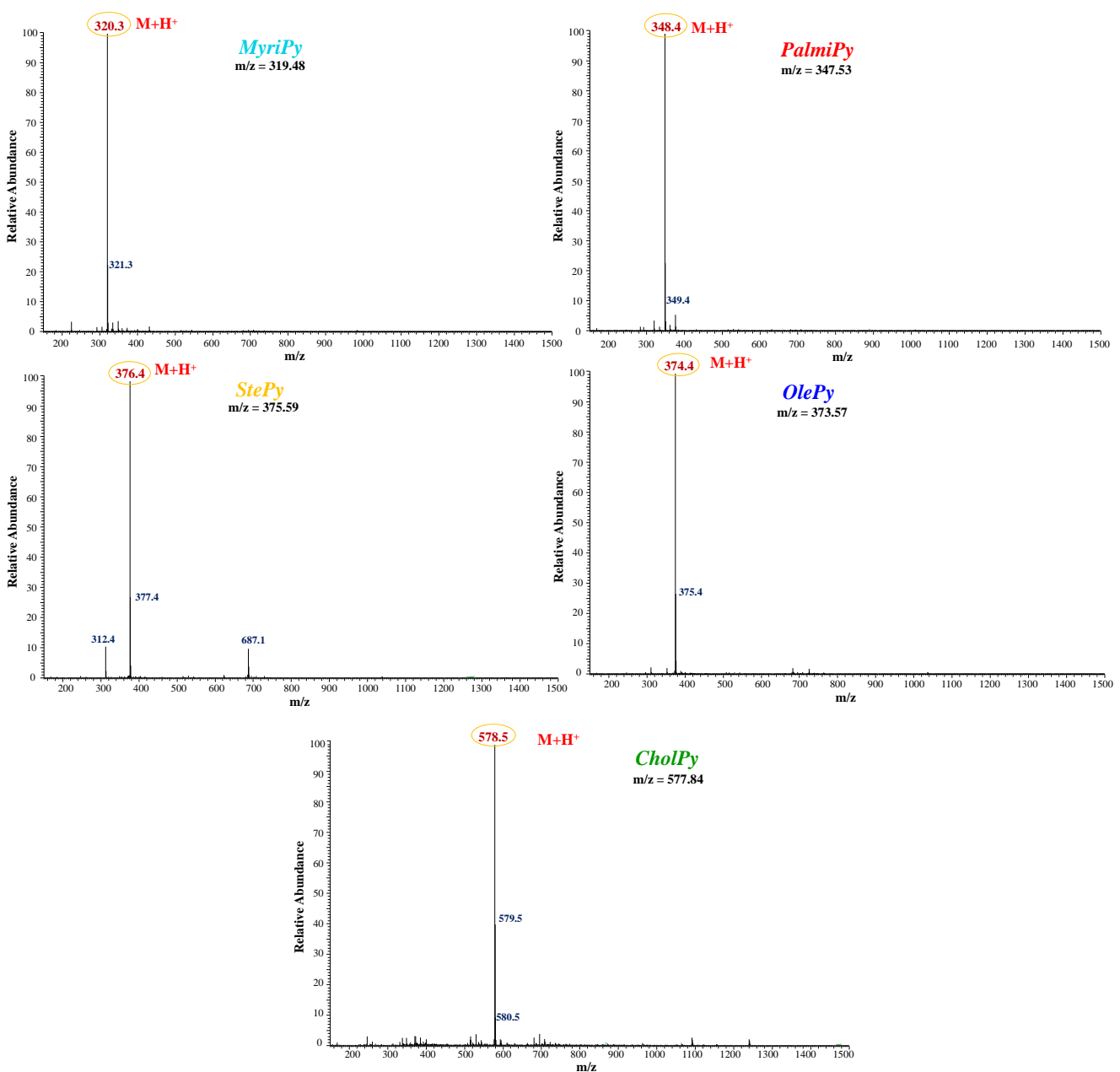


Figure S4. ESI-MS spectra of the here described lipophilic pyridine derivatives recorded in positive ions mode.

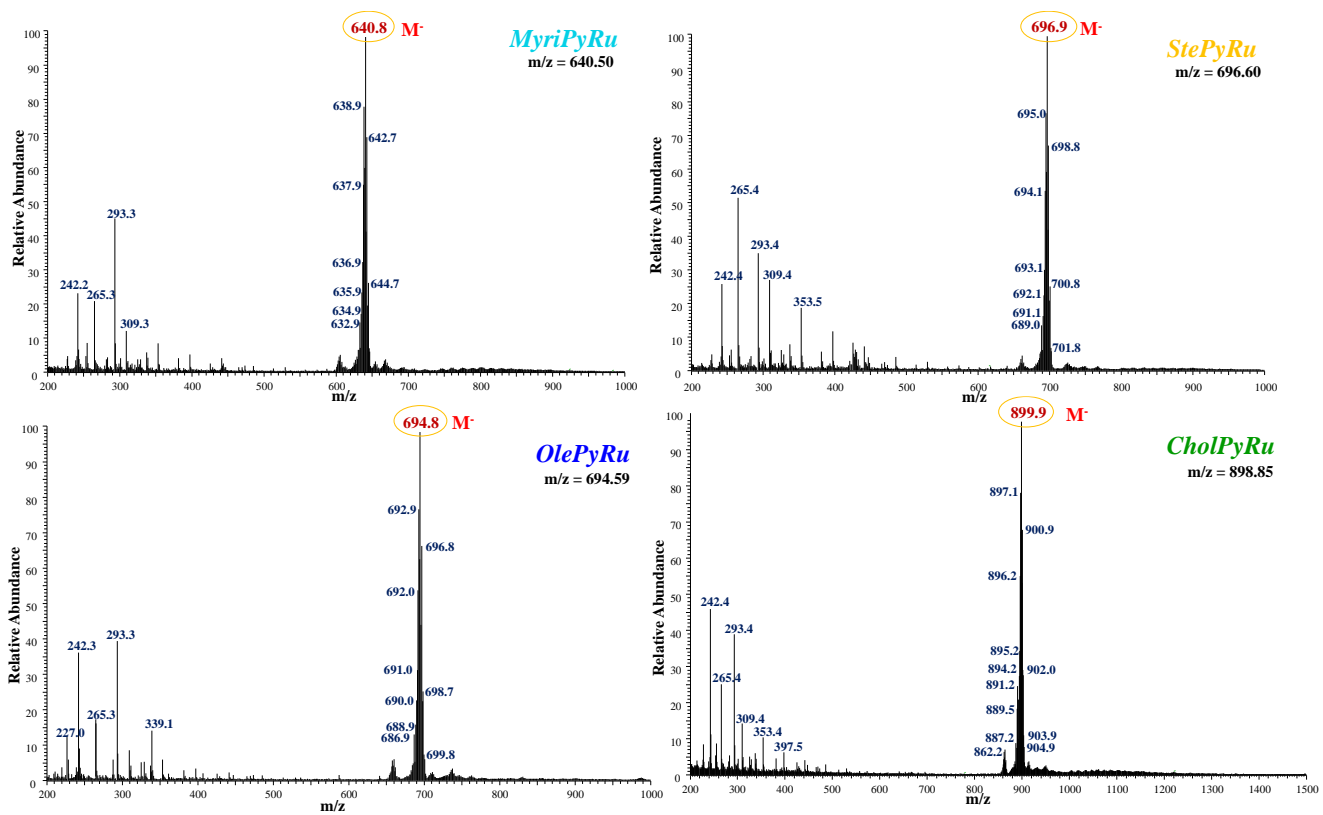


Figure S5. ESI-MS spectra of the here described lipophilic Ru(III) complexes recorded in negative ions mode.

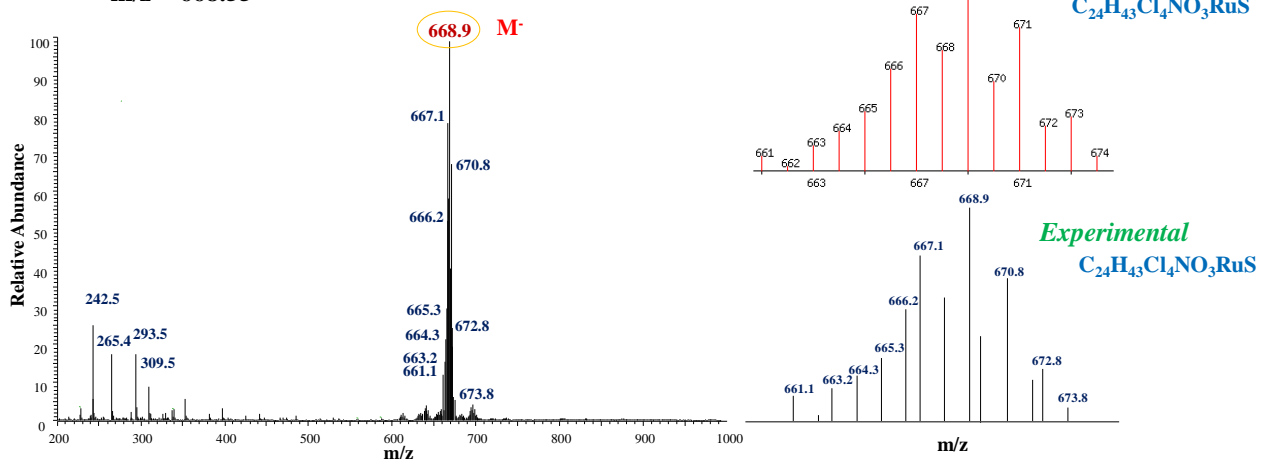
PalmiPyRu**m/z = 668.55**

Figure S6. ESI-MS spectrum of PalmiPyRu recorded in negative ions mode along with the comparison between the peak isotopic distribution experimentally determined and the theoretical one, as calculated using the *Isotope Distribution Calculator* program (<http://www.sisweb.com/mstools/isotope.htm>).

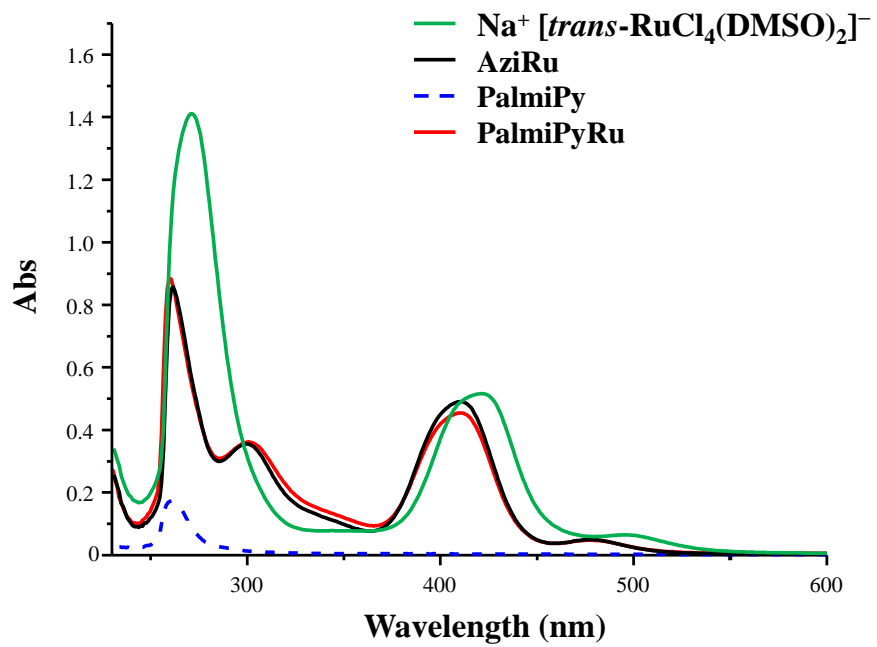


Figure S7. Overlapped UV-vis absorption spectra of freshly dissolved $\text{Na}^+ [\text{trans}-\text{RuCl}_4(\text{DMSO})_2]^-$, AziRu, PalmiPy, and PalmiPyRu (green, black, blue and red lines, respectively) in DMSO at 100 μM concentration.

	λ_{\max} (DMSO)	λ_{\max} (phosphate buffer solution)
AziRu	410 nm	395 nm
MyriPyRu	409 nm	401 nm
PalmiPyRu	410 nm	408 nm
StePyRu	409 nm	401 nm
OlePyRu	410 nm	398 nm
CholPyRu	410 nm	401 nm

Table S1. Wavelength values at the absorbance maxima of the characteristic ligand-to-metal charge transfer (LMCT) band observed for all the analyzed compounds, freshly dissolved in DMSO and in the selected aq. phosphate buffer solution.

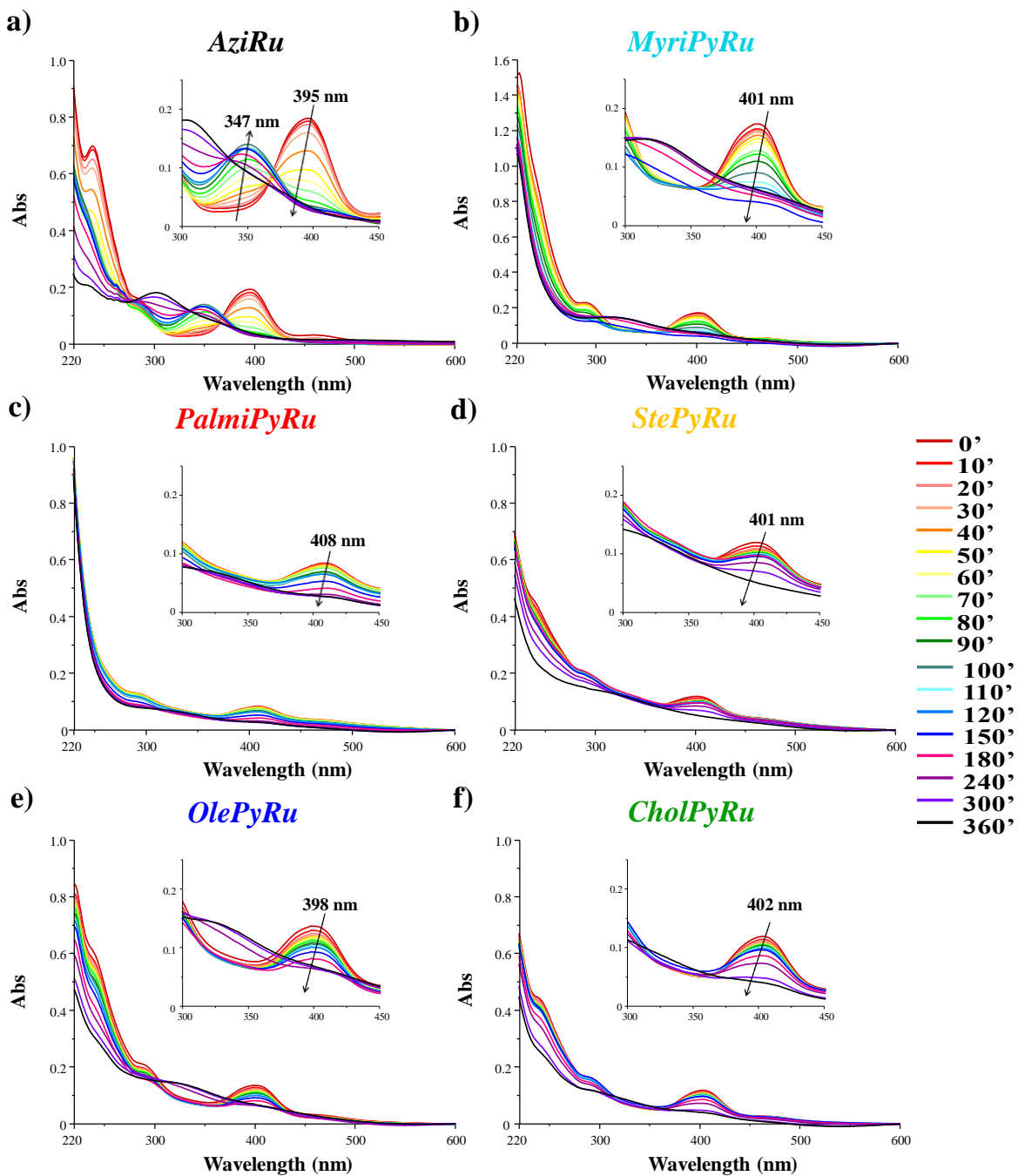


Figure S8. Overlapped UV–vis absorption spectra of (a) AziRu, (b) MyriPyRu, (c) PalmiPyRu, (d) StePyRu, (e) OlePyRu and (f) CholPyRu both at 50 μ M concentration in the saline phosphate buffer solution (10 mM phosphate buffer/100 mM NaCl, pH=7.3), recorded at different times after dissolution (0 → 360 min). In each panel, insets represent an enlargement of UV-vis spectra in the 300–450 nm range highlighting the Abs_{max} observed at time zero.

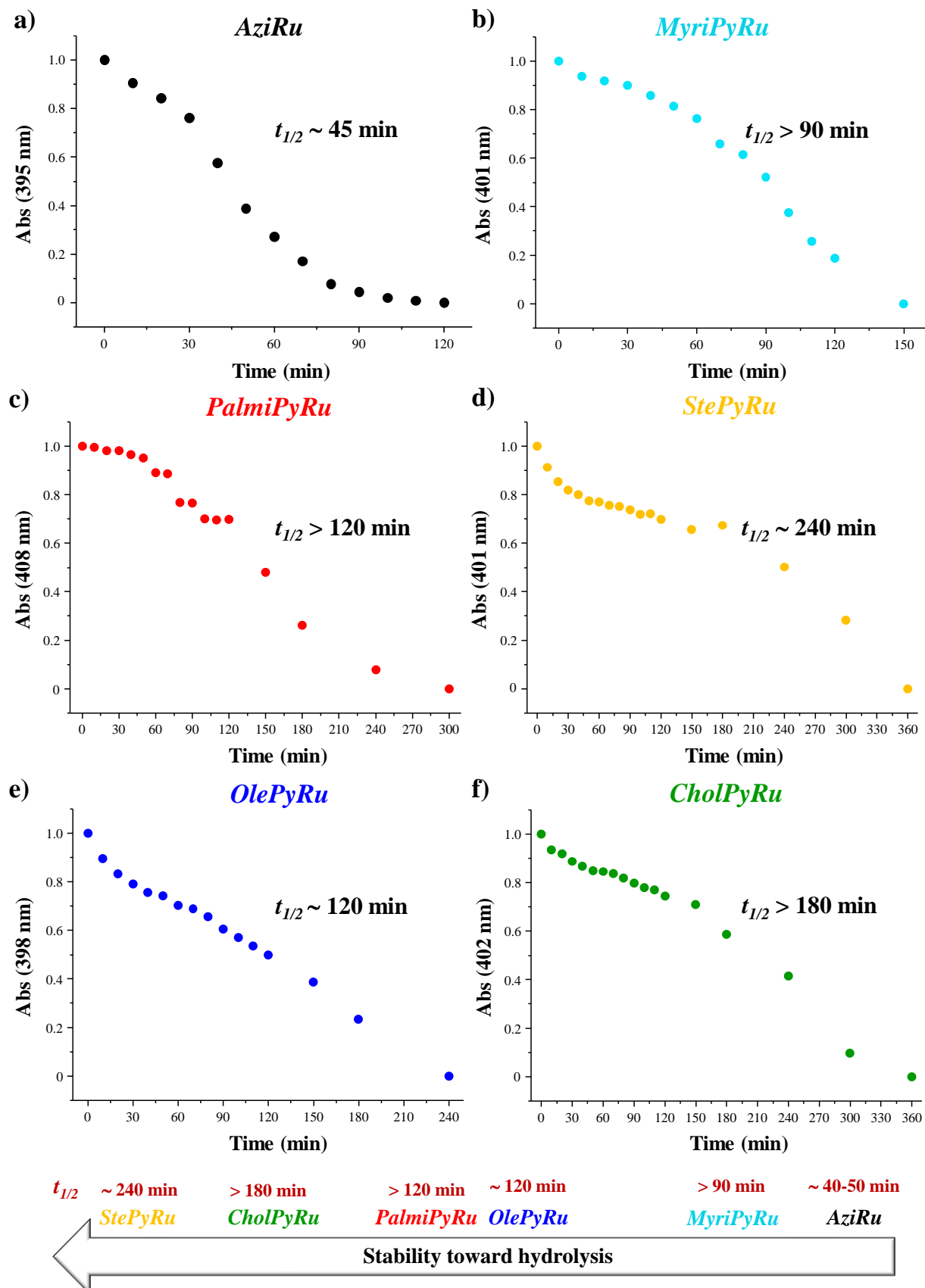


Figure S9. Monitoring of the hydrolysis process over time and evaluation of the $t_{1/2}$ values, as determined by analyzing the changes of the LMCT-band absorbance maxima as a function of time in the selected phosphate buffer solution for: (a) AziRu, (b) MyriPyRu, (c) PalmiPyRu, (d) StePyRu, (e) OlePyRu and (f) CholPyRu.

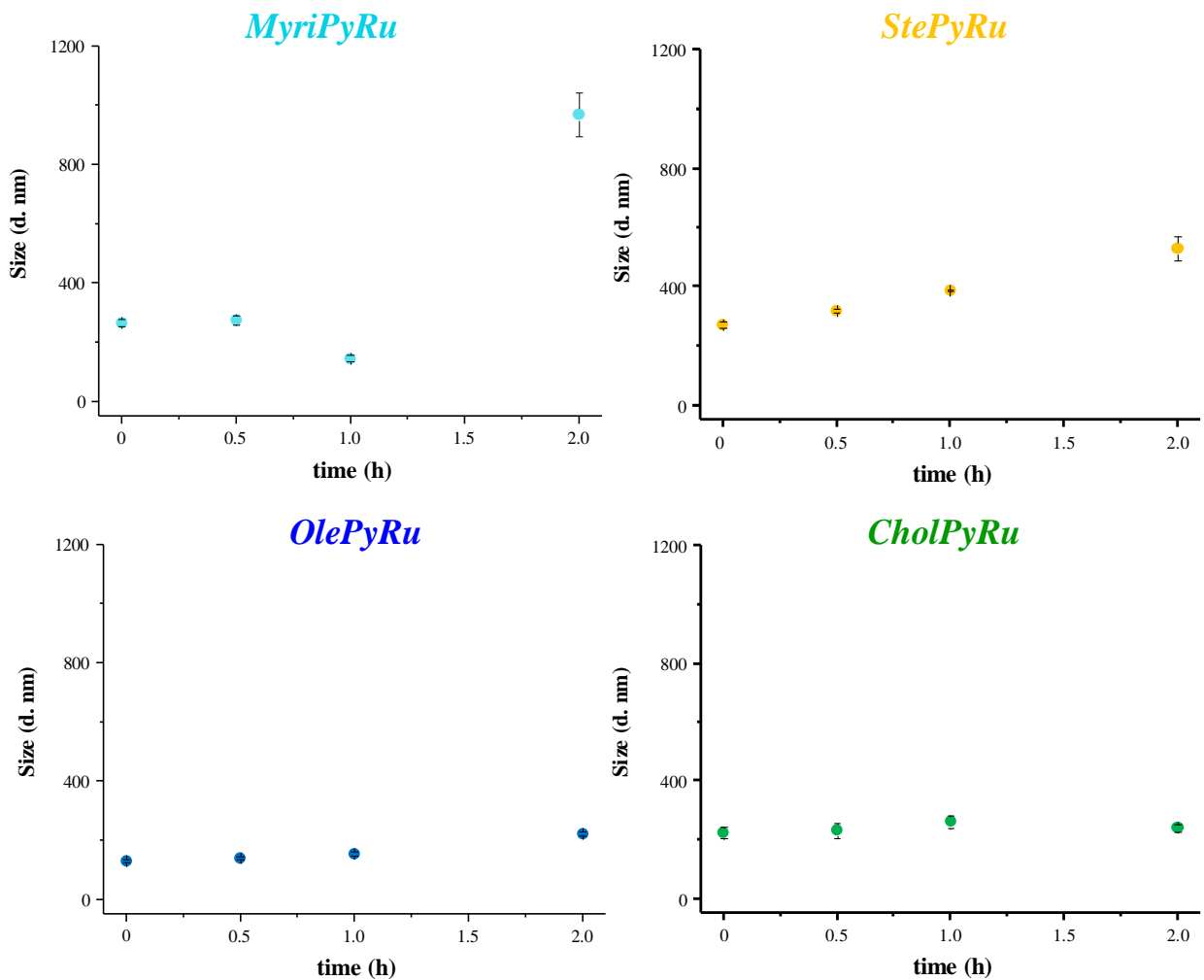


Figure S10. Size (d., nm), determined by DLS analysis, reported as a function of time for MyriPyRu, StePyRu, OlePyRu and CholPyRu, as indicated on top of each graph. Data are reported as mean values \pm SD for multiple determinations.

	MyriPyRu	PalmiPyRu	StePyRu	OlePyRu	CholPyRu
time (h)	Size (d, nm) ± SD				
0	264.9 ± 12.9	272.6 ± 7.6	269.8 ± 11.0	129.2 ± 5.1	222.0 ± 19.1
0.5	274.4 ± 15.9	303.1 ± 71.6	317.5 ± 7.0	139.6 ± 6.0	231.4 ± 25.1
1	144.9 ± 11.2	356.8 ± 18.5	385.7 ± 2.5	153.6 ± 7.7	260.5 ± 21.7
2	968.1 ± 73.3	263.0 ± 12.9	528.2 ± 39.2	221.7 ± 7.6	239.1 ± 13.3
	PdI ± SD				
0	0.51 ± 0.04	0.32 ± 0.01	0.52 ± 0.01	0.25 ± 0.01	0.26 ± 0.02
0.5	0.47 ± 0.01	0.30 ± 0.02	0.46 ± 0.01	0.31 ± 0.02	0.28 ± 0.07
1	0.37 ± 0.03	0.43 ± 0.04	0.43 ± 0.02	0.28 ± 0.03	0.26 ± 0.04
2	0.27 ± 0.05	0.32 ± 0.01	0.37 ± 0.06	0.36 ± 0.02	0.27 ± 0.07

Table S2. Size (d., nm), determined by DLS analysis, and corresponding PdI values reported as a function of time for the studied lipophilic Ru(III) complexes. Data are reported as mean values ± SD for multiple determinations.

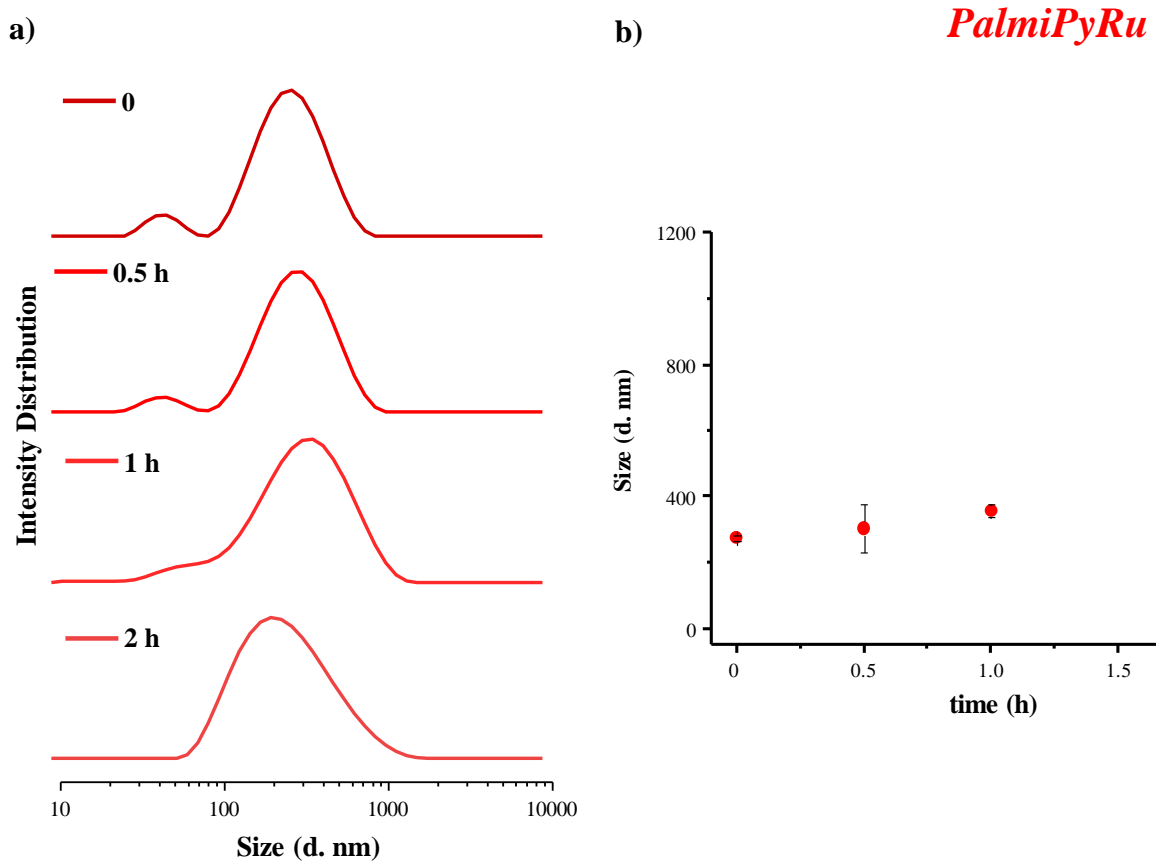


Figure S11. **a)** Size distribution by intensity (d., nm), determined by DLS analysis, of PalmiPyRu at 50 μ M concentration in the selected phosphate buffer solution at different monitoring times, as indicated. **b)** Size (d., nm), determined by DLS analysis, of PalmiPyRu reported as a function of time. Data are reported as mean values \pm SD for multiple determinations.

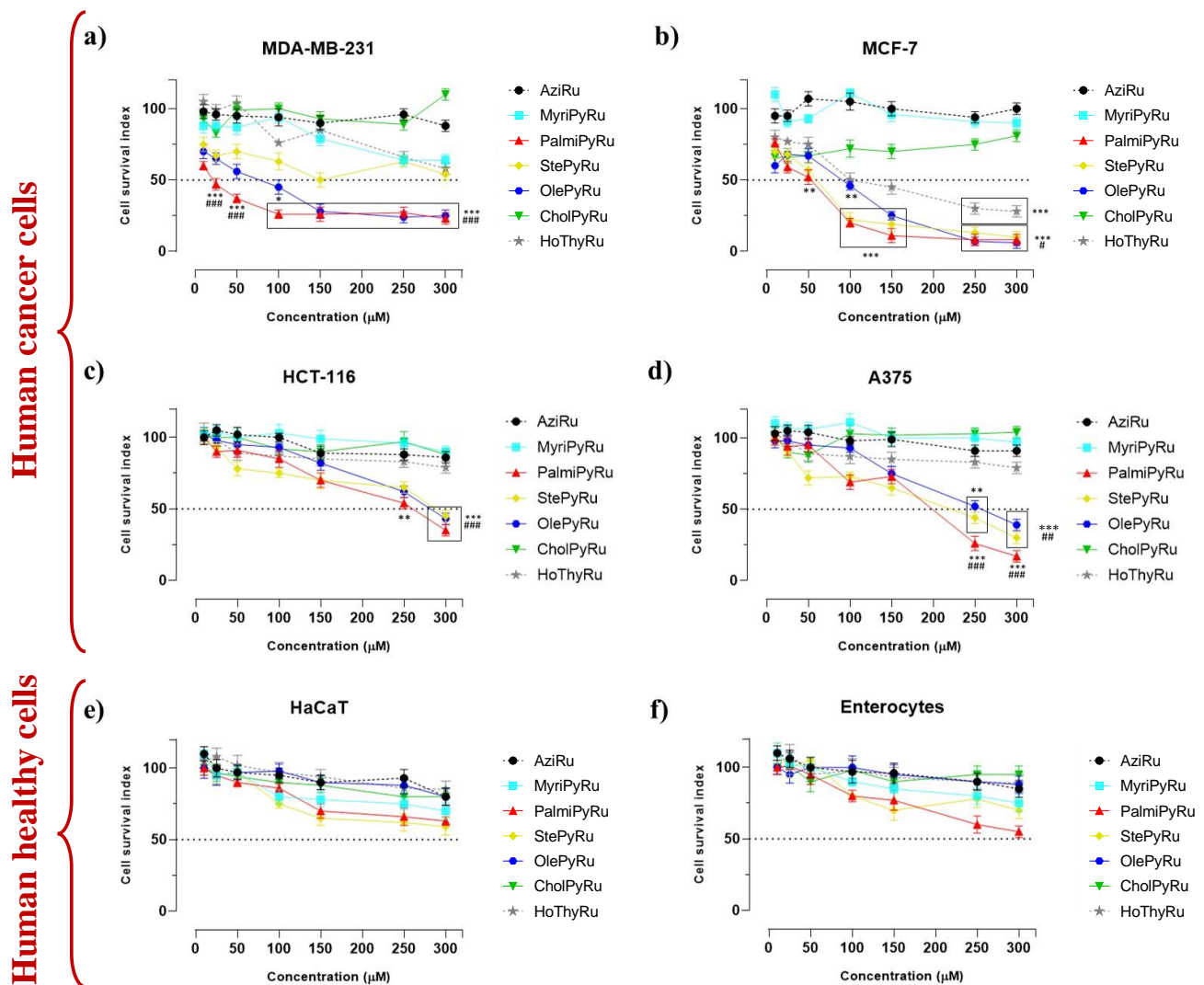


Figure S12. Cell survival index, evaluated by the MTT assay and monitoring of live/dead cell ratio, for **a)** MDA-MB-231, **b)** MCF-7, **c)** HCT-116, **d)** A375, **e)** HaCaT and **f)** enterocytes, following 48 h of incubation with the indicated concentrations ($10 \rightarrow 300 \mu\text{M}$) of AziRu, MyriPyRu, PalmiPyRu, StePyRu, OlePyRu, CholPyRu and HoThyRu, as indicated in the legend. Data are expressed as percentage of untreated control cells and are reported as mean of five independent experiments \pm SEM ($n = 30$). *** $p < 0.001$ vs. untreated cells; ** $p < 0.01$ vs. untreated cells; ### $p < 0.001$ vs. HoThyRu treated cells; ## $p < 0.01$ vs. HoThyRu treated cells; # $p < 0.05$ vs. HoThyRu

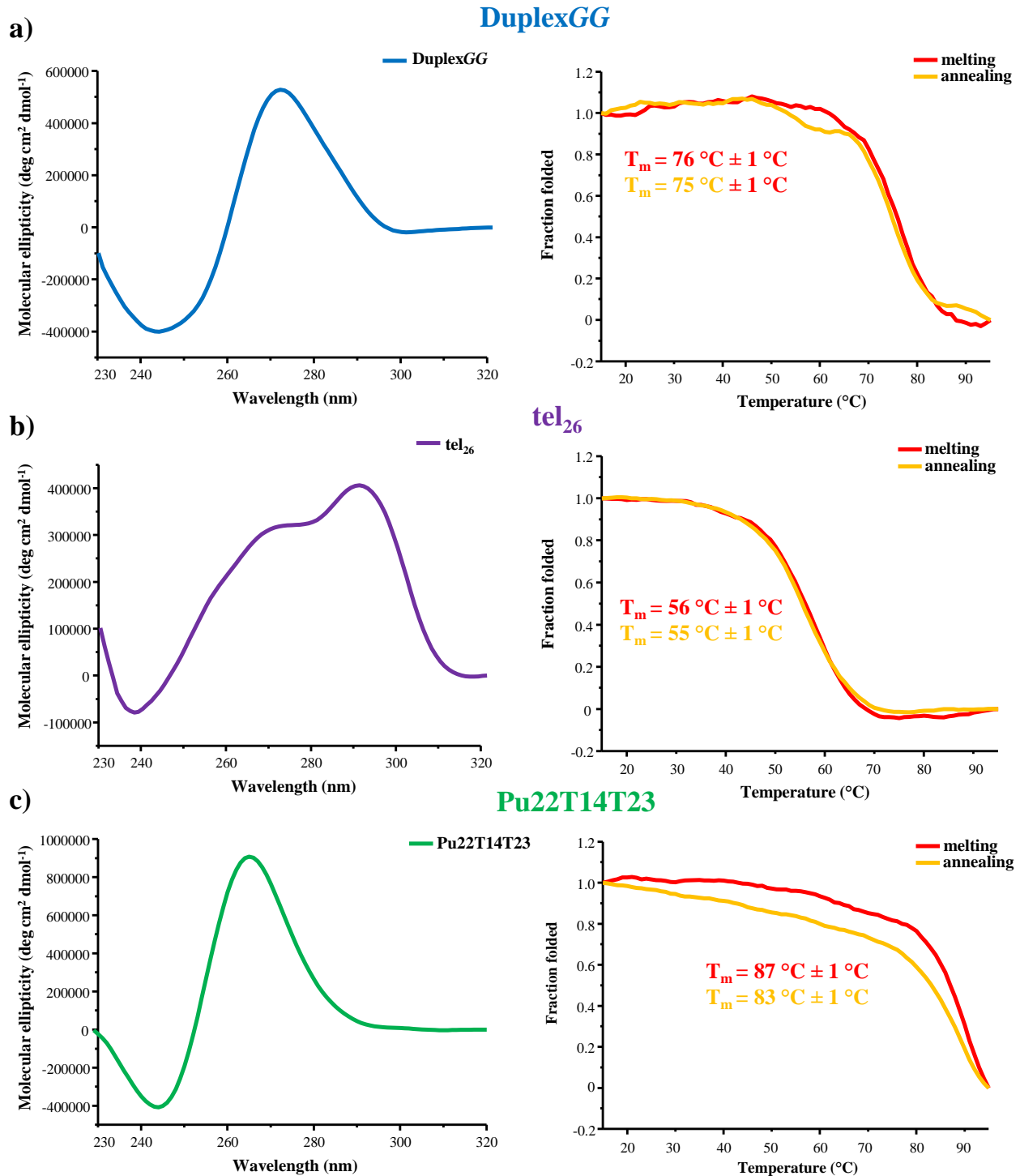


Figure S13. Representative CD spectra at 15 °C (left) and CD-melting/annealing profiles (right) of **a**) duplexGG, **b**) tel₂₆ and **c**) Pu22T14T2 DNA selected as model systems of a hairpin duplex, a telomeric and an oncogene G-quadruplexes, respectively, all analyzed at 2 μM concentration. CD-monitored thermal denaturation/renaturation curves, recorded in the 15–95 °C range at a scan rate of 1.0 °C/min, are reported as folded fraction of each oligonucleotide as a function of temperature.

duplexGG

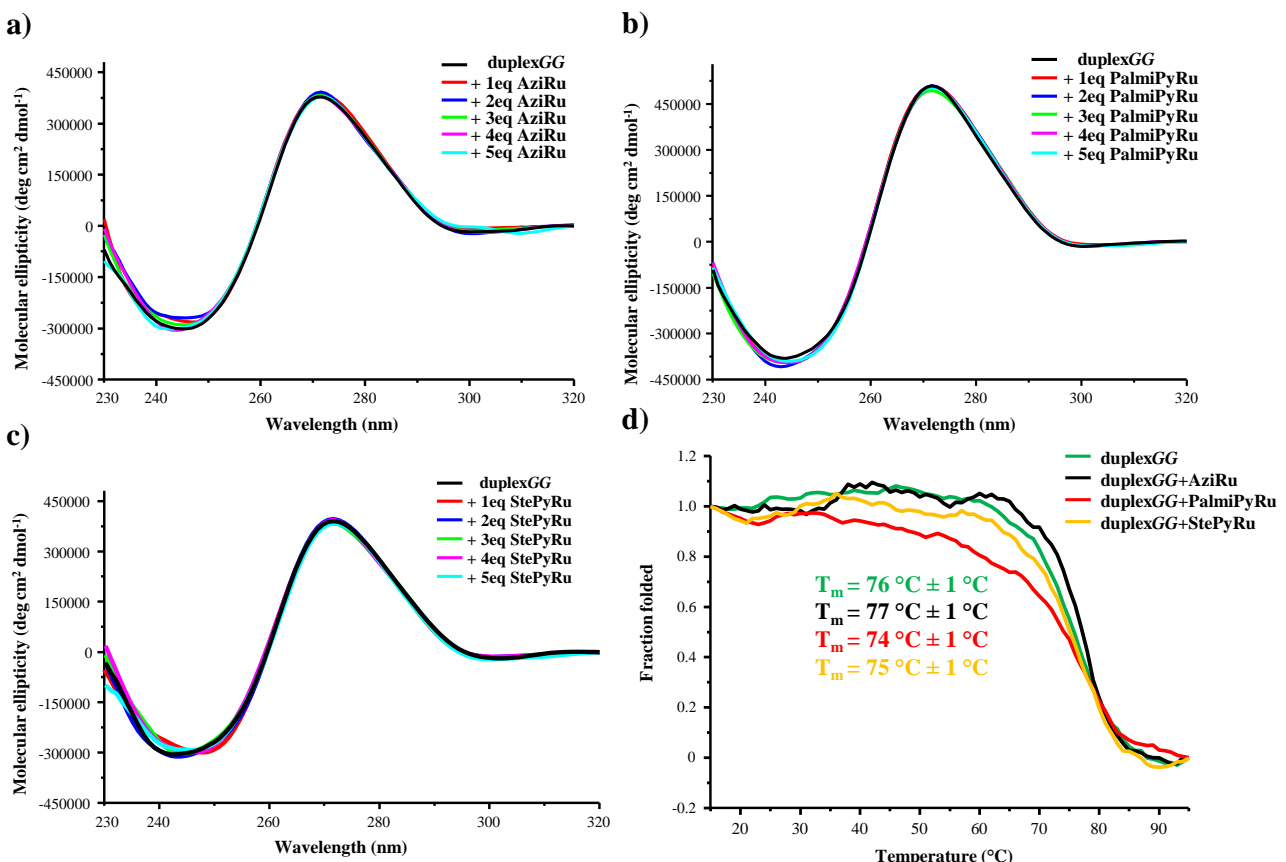


Figure S14. Representative overlapped CD spectra of duplexGG as hairpin duplex model (at 15 °C and 2 μM concentration in the selected K⁺-rich buffer solution), in the absence and presence of increasing equivalents of **a)** AziRu, **b)** PalmiPyRu and **c)** StePyRu. **d)** Representative CD-melting experiments of duplexGG in the absence and presence of 5 equivalents of each Ru(III) complex, as indicated in the legend, reported as folded fraction of the oligonucleotide as a function of temperature. CD-melting curves (monitored at 271 nm) were recorded at 2 μM oligonucleotide concentration in the 15–95 °C range at a scan rate of 1.0 °C/min.

Pu22T14T23

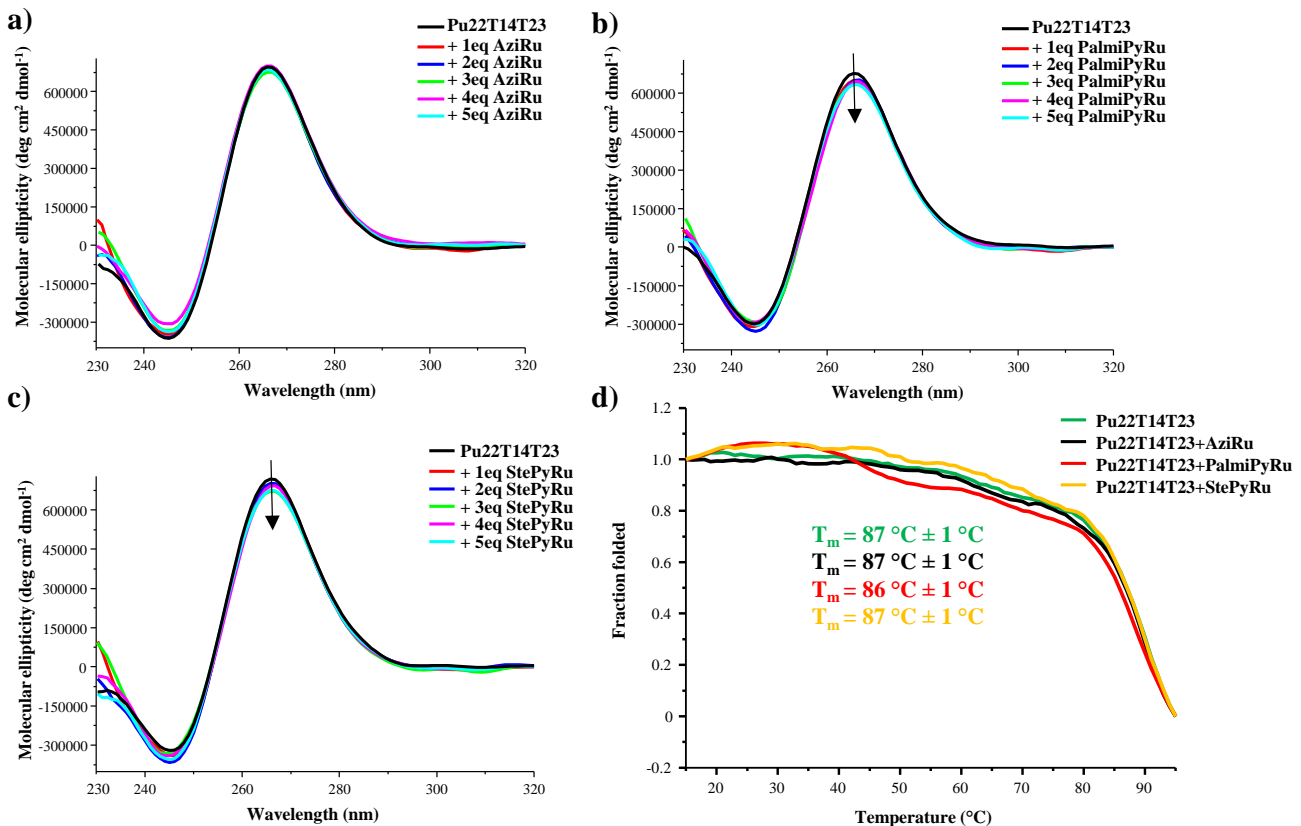


Figure S15. Representative overlapped CD spectra of Pu22T14T23 as oncogene G-quadruplex model (at 15 °C and 2 μM concentration in the selected K⁺-rich buffer solution), in the absence and presence of increasing equivalents of **a)** AziRu, **b)** PalmiPyRu and **c)** StePyRu. **d)** Representative CD-melting experiments of Pu22T14T23 in the absence and presence of 5 equivalents of each Ru(III) complex, as indicated in the legend, reported as folded fraction of the oligonucleotide as a function of temperature. CD-melting curves (monitored at 265 nm) were recorded at 2 μM oligonucleotide concentration in the 15–95 °C range at a scan rate of 1.0 °C/min.

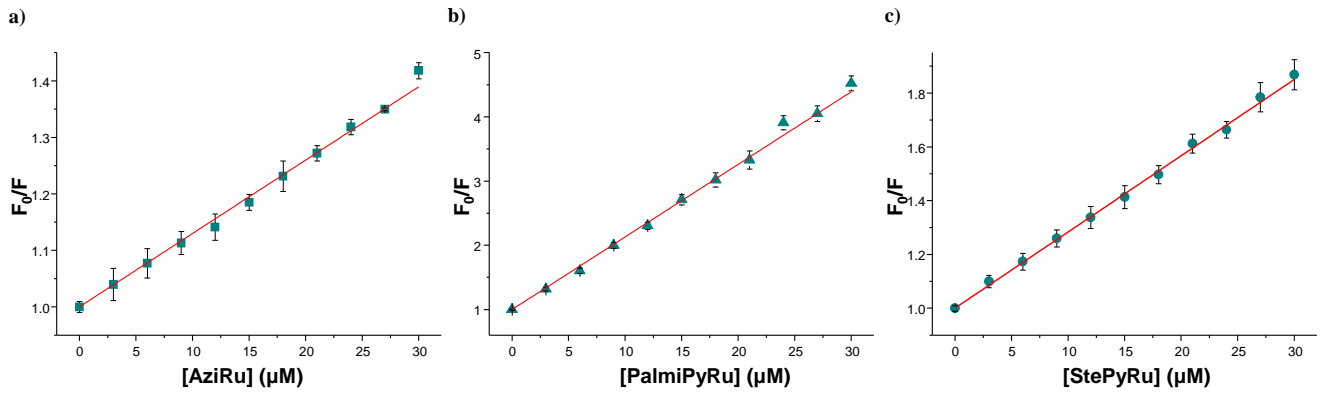


Figure S16. Stern-Volmer plots for the interaction of: **a)** AziRu, **b)** PalmiPyRu and **c)** StePyRu with BSA at 20 °C. Data are reported as mean values \pm SD for multiple determinations. Solid red lines represent the best linear fit of the data.

Sample	r^2	K_{sv} (M^{-1})	kq ($M^{-1} s^{-1}$)
AziRu	0.99998	1.3×10^4	1.3×10^{12}
PalmiPyRu	0.99957	1.1×10^5	1.1×10^{13}
StePyRu	0.99994	2.8×10^4	2.8×10^{12}

Table S3. Stern-Volmer quenching constants (K_{sv}) and bimolecular quenching rate constants (kq) for the titration experiments of BSA (3 μM in PBS buffer) with AziRu, PalmiPyRu and StePyRu at 20 °C. Errors on K_{sv} and k_q determination are ca. $\pm 10\%$. The correlation coefficient (r^2) is obtained by the linear fit of the data reported in Figure S14.

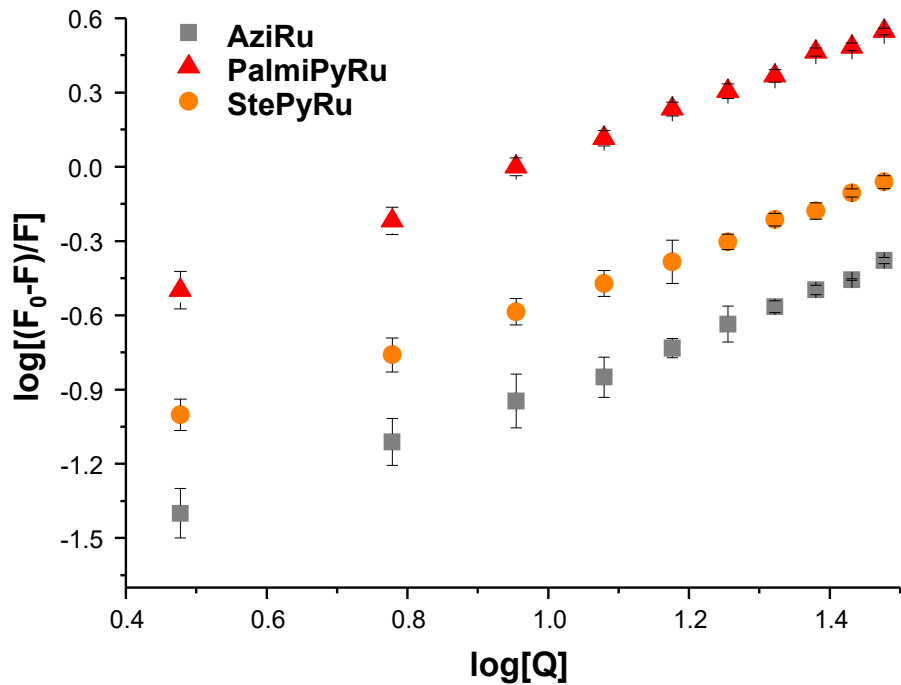


Figure S17. Overlapped double logarithmic plots for the quenching of BSA fluorescence caused by interaction with the tested Ru(III) compounds, as indicated in the legend. Data are reported as mean values \pm SD for multiple determinations.

Sample	r^2	K_b (M⁻¹)	n
AziRu	0.975	1.08 x 10 ⁴	1.06
PalmiPyRu	0.995	9.54 x 10 ⁴	1.06
StePyRu	0.996	3.11 x 10 ⁴	0.98

Table S4. Apparent binding constants (K_b) and number of binding sites (n) for the titration experiments of BSA (3 μ M in PBS buffer) with AziRu, PalmiPyRu and StePyRu at 20 °C. Errors on K_b determination are ca. \pm 5%. r^2 is the correlation coefficient obtained by the linear fit of the data reported in Figure S17.

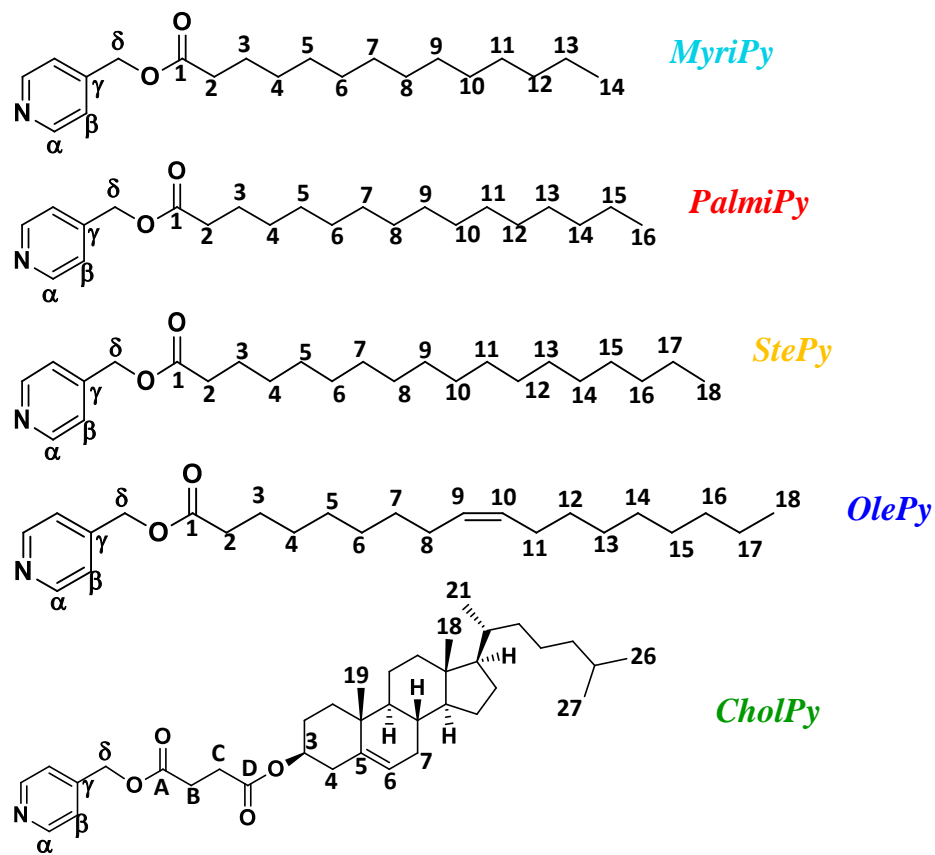


Figure S18. Nomenclature used in the description of NMR spectra to easily identify proton and carbon signals.

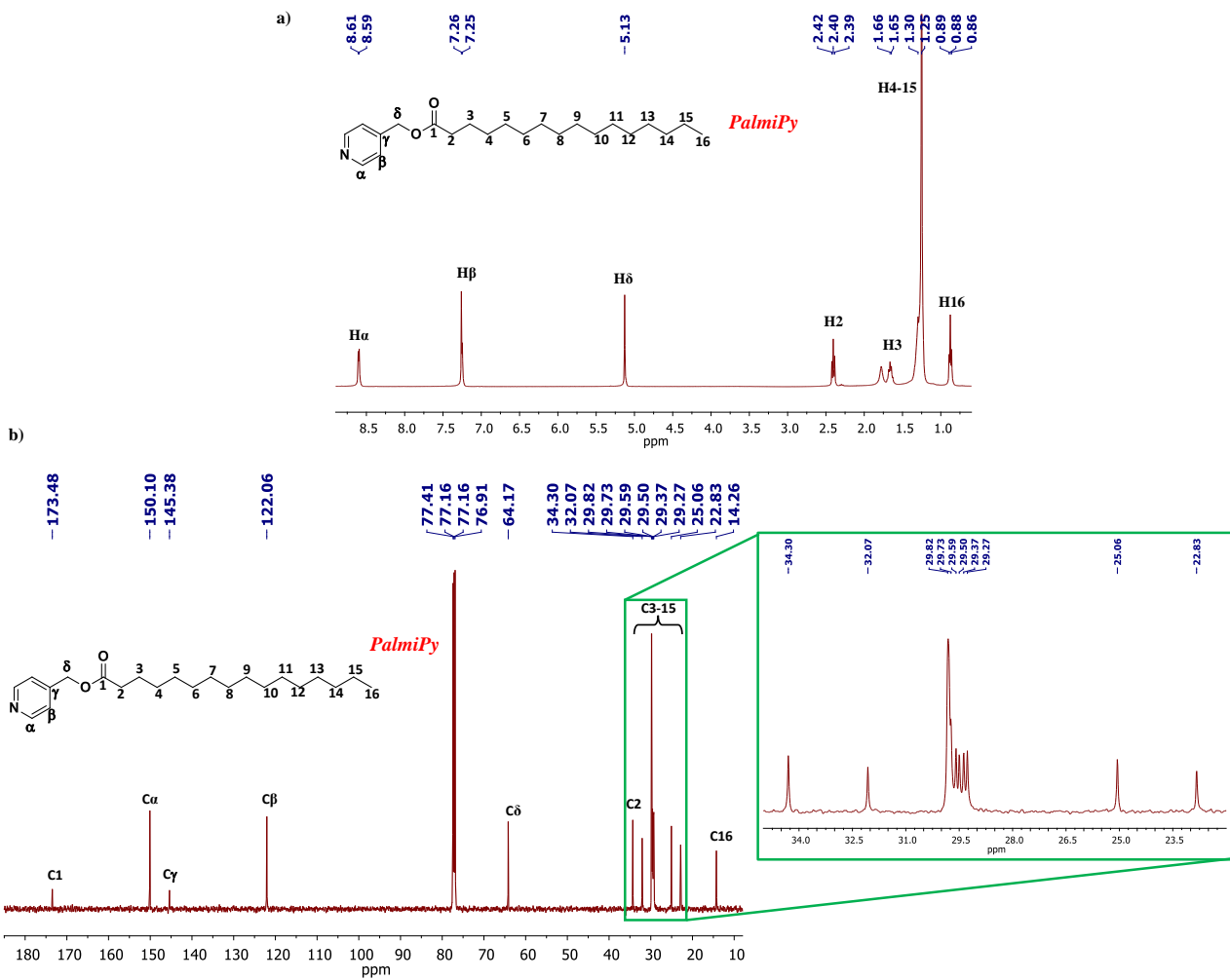


Figure S19. ^1H (400 MHz, **a**) and ^{13}C (125 MHz, **b**) NMR spectra of PalmiPy in CDCl_3 . In panel b, an enlargement (green box) of the 23–35 ppm area of the ^{13}C NMR spectrum is also reported.

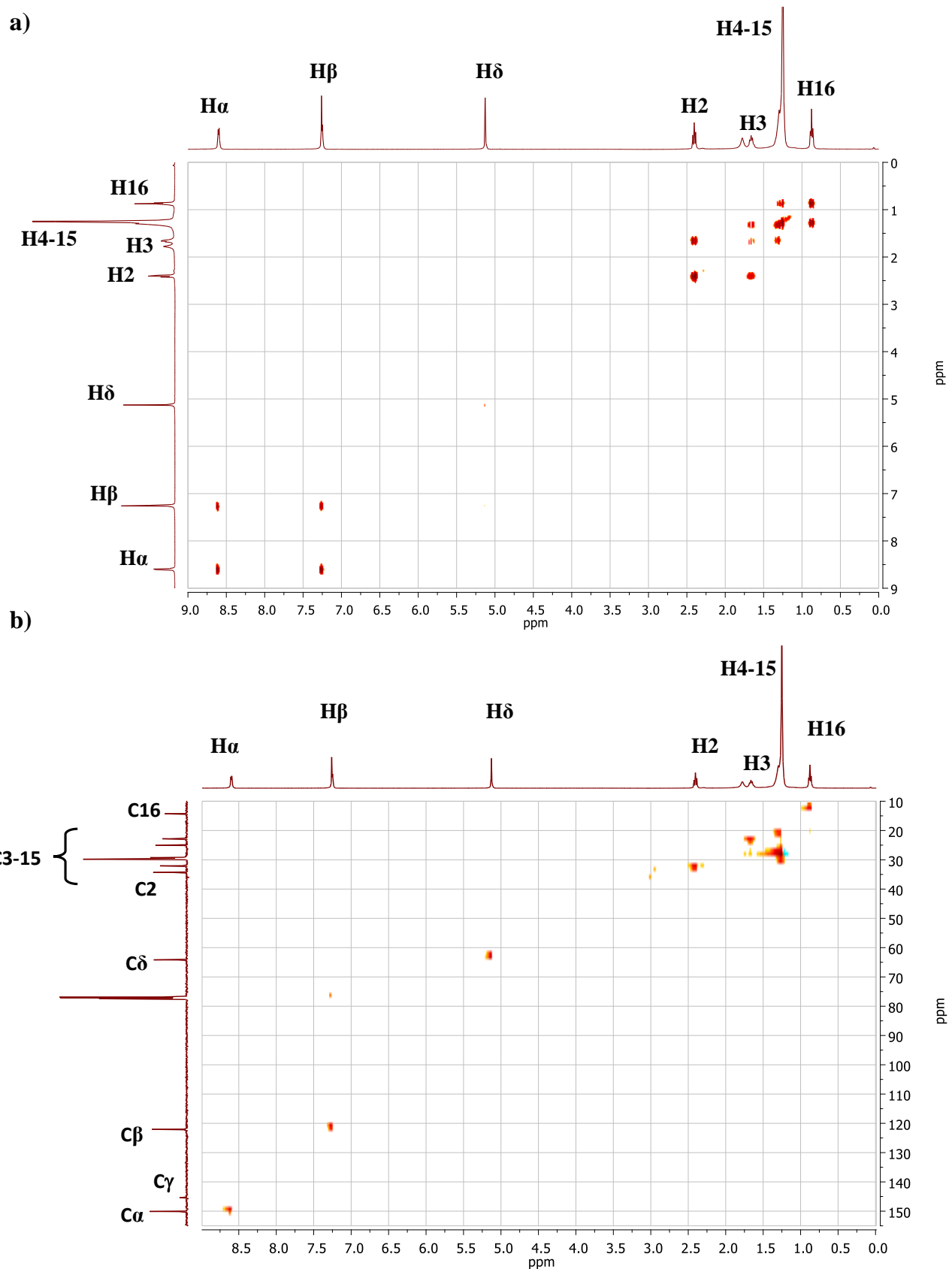


Figure S20. ^1H - ^1H COSY (a) and HSQC (b) NMR spectra (400 MHz) of PalmiPy in CDCl_3 .